Received: 30 June 2020

DOI: 10.1002/mma.6777

SPECIAL ISSUE PAPER

WILEY

Theoretical aspects of micropolar nanofluid flow past a deformable rotating cone

Anber Saleem[1,2] | **Wajiha Sabih**[3] | **Sohail Nadeem**[3] | **Mehdi Ghalambaz**[4,5] | **Alibek Issakhov**[6]

[1]Mathematics and its Applications in Life Sciences Research Group, Ton Duc Thang University, Ho Chi Minh City, Vietnam

[2]Faculty of Mathematics and Statistics, Ton Duc Thang University, Ho Chi Minh City, Vietnam

[3]Department of Mathematics, Quaid-i-Azam University, 45320, Islamabad, 44000, Pakistan

[4]Institute of Research and Development, Duy Tan University, Da Nang, 550000, Vietnam

[5]Faculty of Electrical – Electronic Engineering, Duy Tan University, Da Nang, 550000, Vietnam

[6]Faculty of Mechanics and Mathematics, Al-Farabi Kazakh National University, av. al-Farabi 71, 050040, Almaty, Kazakhstan

Correspondence
Mehdi Ghalambaz, Duy Tan University, Da Nang 550000, Vietnam.
Email: mehdighalambaz@duytan.edu.vn

The intension of this investigation is to analyze the laminar boundary layer flow of micropolar nanofluid inside a deformable rotating cone. A comparison is carried out between three types of nanofluids with nanoparticles, that is, metal (Cu), metallic oxide (Al_2O_3), and a semiconductor (TiO_2) with water as base fluid. Brinkman and Maxwell's model of effective dynamic viscosity and thermal conductivity is considered. Using suitable similarity transformations, the governing coupled non-linear boundary layer partial differential equations are reduced to non-linear ordinary differential equations, which are further solved numerically by bvp4c technique. The results obtained reveal interesting effects of important pertinent parameters, that is, rotation parameter ω, nanoparticle concentration parameter ϕ, and micropolar parameter Δ on velocity, microrotation, and temperature profiles, which are analyzed graphically. A comparative analysis of the results of numerically calculated skin friction coefficients and Nusselt number for these parameters are also presented. The problem throughout the whole study is analyzed for both the strong and weak concentration of micro-elements. It is found that the ω and Δ enhance the flow and ω, ϕ, and Δ boosts the rate of heat transfer in all cases of stretching/shrinking rotating cone except for the case of shrinking rotating cone in which the growth of Δ declines the rate of heat transfer for strong/weak concentration of microelements. Moreover, Cu–*water* has the highest skin friction and Nusselt number.

KEYWORDS

micropolar fluid, nanofluid, rotating cone, stretching/shrinking surface

1 | INTRODUCTION

In fluid dynamics, heat transfer characteristics of rotating surfaces has been an interesting subject of research for a long time as it is widely used in many practical applications such as in rotating machinery, turbo-machinery, and aerodynamic engineering. Due to the rotation of an axisymmetric body in a fluid, heat transfer by the process of convection occurs between the surface of the body and the fluid in contact with it, which helps in the cooling of the system. This phenomenon is useful for many practical applications. Therefore, the focus of this study is to scrutinize the heat transfer mechanism from the surface of the rotating cone when the surface of the cone is subjected to stretching/shrinking while considering micropolar effects and three types of nanofluids in a viscous medium.

It is well known from the previous studies that the problem of rotating cone in a still fluid under boundary layer approximations is similar to the rotating disk problem, which is the special case of rotating cone for vertical cone angle.[1–4] The problem of the rotating disk was first examined by Von Karman for steady, incompressible Newtonian fluid in which he used similarity transformations to solve the laminar boundary layer equations. Similar transformations are used by many researchers to solve rotating cone and stretching or shrinking rotating disk problems. For example, laminar flow and heat transfer over a rotating cone were investigated by Tien,[2] Tien and Tsuji,[3] and by Hering and Grosh.[4] Unsteady mixed convection flow from a vertical rotating cone when a magnetic field is applied to it was examined by Takhar et al.[5] The boundary layer analysis on axisymmetric surfaces, rotating cones, and disks while considering heat source was studied by Wang.[6] Analysis of the viscous flow over a stretchable rotating disk was carried out by Fang.[7] The rate of heat transfer through a rotating disk with a stretchable surface when a magnetic field is applied to it was analyzed by Turkyilmazoglu.[8] The rate of heat transfer due to a shrinking rotating disk when a magnetic field is applied to it was incorporated by Turkyilmazoglu,[9] and many other investigations have been carried out related to these topics.

For cooling industrial appliances, the heat transfer rate of the conventional fluids such as water, engine oil, and ethylene glycol is enhanced by the addition of nanometer-sized particles in these fluids, and the resulting mixture was given the name nanofluid by Choi.[10] Compared to conventional fluids, the thermal conductivity of nanofluids is significantly enhanced due to nanoparticles, but it depends on many factors such as particle size, particle material, particle volume fraction, particle shape, temperature, and base fluid properties. The two most commonly used models to analyze the heat transfer characteristics of nanofluids are the Buongiorno model[11–13] and the nanofluid phase flow model.[14–17] Buongiorno model is concerned with the seven main slip mechanisms between fluid and solid phases such as Brownian diffusion, inertia, thermophoresis, diffusiophoresis, gravity, Magnus effect, and fluid drainage among which Brownian diffusion and thermophoresis are two most prominent mechanisms in the absence of turbulency.[11–12] Hybrid nanofluids are a novel type of nanofluid, which is a composite of two or more nanoparticles.[14–16] Moreover, the nanoparticles can be made of phase change material and form a phase change suspension.[18–20]

The fluid flow phenomena at the micro-scale level are different from that at the macro-scale level due to which the Navier–Stokes equation, which is derived from classical continuum becomes incapable of explaining such flows in which the effect of molecular spin needs to be considered. Therefore, Eringen[21] developed micro continuum theory to account for such micro-motions in which each finite-size particle can rotate and deform independently. The effect of such local rotations (micro-motions) of the micro-structures is added with the usual motion of the fluid. Three additional degrees of freedom (named as gyration vector) are considered to account for the initial characteristics of the micro-structures (local rotations), and the law of conservation of angular momentum is added to the laws of conservation in classical fluid mechanics to take into account these microscopic effects that are arising from the intrinsic motion of the fluid particles.[22,23] Willson,[26] Ahmadi,[27] Chamkha et al.,[28] and Peddieson[29] discussed boundary layer approximation for micropolar fluids. Micropolar fluid theory helps in providing the mathematical model for the non-Newtonian fluid behavior, which is exhibited by polymeric fluids, muddy fluids, biological fluids, and anisotropic fluids like liquid crystal with rigid molecules.[21–33] Physically, micropolar fluids consist of randomly oriented, rigid spherical particles suspended in a viscous medium that can support body couples, couple stresses, and a non-symmetric stress tensor.[17,21] In micropolar fluids, the macroscopic velocity field is coupled with the particle rotational motion, and vortex viscosity acts as a coupling constant. Chamkha et al.[28] Nawaz,[31] and Rashad et al.[32] presented researches on different flows in micropolar fluids. The rotating disk problem in a micropolar fluid was studied by Guram and Anwar.[33] Stretchable rotating disk problem in the micropolar fluid was analyzed by Hussain and Kamal.[34] Postelnicu,[35] Takhar et al.,[36] and Cheng[37,38] discussed the vertical cone problem in a micropolar fluid. Rotating cones in micropolar fluids were analyzed by Gorla and Nakamura,[39] Eldahab and Aziz,[40] Gorla and Nakamura.[41] Ahmed[42] discussed vertical permeable cone problem in a micropolar nanofluid, but the cone was neither subjected to rotation nor could undergo stretching or shrinking. The author concluded that as vortex viscosity increases, velocity profile, as well as Nusselt number decreases and the most prominent effect was for copper nanoparticles. Other studies in which micropolar nanofluid flow over a stretchable surface is considered were conducted by Gorla and Takhar [41] Hussain et al.,[43] and Subhani and Nadeem.[44]

In view of the above researches, we can conclude that the horizontal deformable rotating cone in a micropolar nanofluid has not been studied yet. Therefore the main goal of this research is to investigate the dynamic and thermal characteristics of a deformable rotating cone, when the cone wall can undergo stretching or shrinking in a micropolar nanofluid. The micro-rotational effects are considered in the equation of motion, and the law of conservation of angular momentum is added to the basic laws of motion in classical fluid mechanics. Heat transfer analysis for three types of nanofluids Cu,Al_2O_3, and TiO_2 with water as a base fluid is carried out considering the flow to be steady, incompressible, and axisymmetric laminar boundary layer flow. Effects of rotation parameter, nanoparticles volume fraction

parameter, and micropolar parameter on velocity, temperature, and micro-rotation profiles are displayed through graphs, and on skin friction coefficients and Nusselt number are computed numerically in tabular form which is presented in Section 4.

2 | MATHEMATICAL MODELING

This study involves horizontal deformable cone, rotating in an infinite medium with constant angular frequency Ω in a quiescent micropolar nanofluid. Water as a base fluid and metal (Copper Cu), metallic oxide (alumina Al_2O_3), and a semi-conductor (titania TiO_2) as nanoparticles are considered to be in thermal equilibrium, and no-slip occurs in between them. The flow with constant fluid properties (density, viscosity, thermal conductivity, etc.) is considered under a rectangular fixed coordinate system (r, θ, z), as shown in Figure 1, where the axis r is along the meridional section, θ along the circular cross-section, and z normal to the surface of the cone. Equations of motion for isotropic micropolar nanofluid are given as follows[15,20,21,28,31]:

$$\frac{\partial \rho_{nf}}{\partial t} + \left(\mathbf{V}^* \cdot \boldsymbol{\nabla}\right)\rho_{nf} + \rho_{nf}\left(\boldsymbol{\nabla} \cdot \mathbf{V}^*\right) = 0, \tag{1}$$

$$\begin{aligned}\rho_{nf}\left[\frac{\partial \mathbf{V}^*}{\partial t} + \left(\mathbf{V}^* \cdot \boldsymbol{\nabla}\right)\mathbf{V}^*\right] &= \left(\zeta + 2\mu_{nf} + \varkappa\right)\boldsymbol{\nabla}\left(\boldsymbol{\nabla} \cdot \mathbf{V}^*\right) + \varkappa(\boldsymbol{\nabla} \times \mathbf{N}) \\ &\quad - \left(\mu_{nf} + \varkappa\right)\left(\boldsymbol{\nabla}\left(\boldsymbol{\nabla} \cdot \mathbf{V}^*\right) - \boldsymbol{\nabla}^2\mathbf{V}^*\right) - \boldsymbol{\nabla}P + \rho_{nf}f,\end{aligned} \tag{2}$$

$$\begin{aligned}\rho_{nf}j\left[\frac{\partial \mathbf{N}}{\partial t} + \left(\mathbf{V}^* \cdot \boldsymbol{\nabla}\right)\mathbf{N}\right] &= \left(\chi + \beta + \gamma_{nf}\right)\boldsymbol{\nabla}(\boldsymbol{\nabla} \cdot \mathbf{N}) - \gamma_{nf}\left(\boldsymbol{\nabla}(\boldsymbol{\nabla} \cdot \mathbf{N}) - \boldsymbol{\nabla}^2\mathbf{N}\right), \\ &\quad + \varkappa\left(\boldsymbol{\nabla} \times \mathbf{V}^* - 2\mathbf{N}\right) + \rho_{nf}l\end{aligned} \tag{3}$$

$$\left(\rho C_p\right)_{nf}\left[\frac{\partial T}{\partial t} + \left(\mathbf{V}^* \cdot \boldsymbol{\nabla}\right)T\right] = k_{nf}\left(\boldsymbol{\nabla}^2 T\right) + \Phi, \tag{4}$$

where the dissipation function Φ in case of micropolar fluid is[21,29]

$$\Phi = \boldsymbol{\tau}^* : \left(\boldsymbol{\nabla}\mathbf{V}^* - \boldsymbol{\varepsilon} \cdot \mathbf{N}\right) + \mathbf{C} : \boldsymbol{\nabla}\mathbf{N} = t_{st}\left(v_{t,s} + \varepsilon_{tsv}\pi_v\right) + m_{st}\pi_{t,s.} \tag{5}$$

$\boldsymbol{\tau}^*$,$\mathbf{V}^*$,$\mathbf{N}$, and $\mathbf{C}$ represent stress tensor, velocity vector, micro-rotation vector (gyration vector), and couple stress tensor, respectively, and these are the dyadic notations (non-suffix notation) for t_{st},v_t, and π_v, and m_{st}.$\boldsymbol{\varepsilon}$ or ε_{tsv} is the alternating tensor of Levi-civita. ρ_{nf},$(\rho C_p)_{nf}$,ζ,k_{nf},μ_{nf},P,$\varkappa$,j,f,l, and T symbolize density of nanofluid, heat capacitance of nanofluid, second coefficient of viscosity (bulk viscosity), thermal conductivity of nanofluid, dynamic viscosity of nanofluid, pressure, vortex viscosity, micro-inertia density per unit mass, body forces, body couples per unit mass, and temperature,

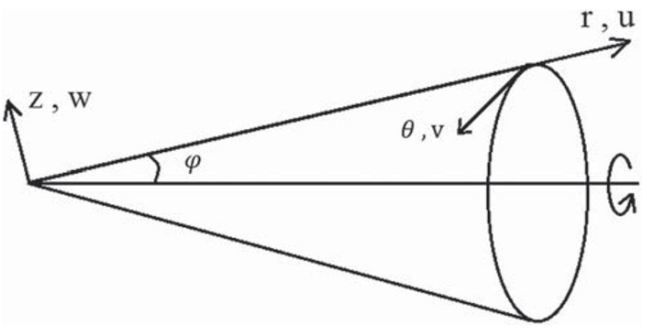

FIGURE 1 The physical configuration of the flow

respectively. χ,β, and γ are known as gyro viscosity coefficients.[28,29] The constitutive equations for micropolar fluid introduced by Eringen are[21,28,29,31]

$$t_{st} = (-P + \zeta v_{r,r})\,\delta_{st} + \mu(v_{s,t} + v_{t,s}) + \varkappa(v_{t,s} - \varepsilon_{stv}\pi_v)\; m_{st} = \chi\pi_{r,r}\delta_{st} + \beta\pi_{s,t} + \gamma\pi_{t,s}, \tag{6}$$

where δ_{st} is Kronecker delta and the material constants ζ,μ,ϰ,χ,β,γ are related by the inequalities as[20,28,29,31]

$$3\zeta + \varkappa + 2\mu \geq 0,\ \varkappa + 2\mu \geq 0,\ 3\chi + \beta + \gamma \geq 0,\ \varkappa \geq 0,\ \gamma \geq 0,\ \gamma \geq |\beta|. \tag{7}$$

The fluid flow is assumed to be steady, axisymmetric, incompressible laminar boundary layer flow. The components of $\mathbf{V}^*$ and $\mathbf{N}$ are chosen of the form

$$\mathbf{V}^* = [u(r,z), v(r,z), w(r,z)], \mathbf{N} = [0, N(r,z), 0].$$

The field equations after substituting velocity vector and micro-rotation vector components are reduced to boundary layer partial differential equations on the basis of the order of magnitude analysis in which the terms of order δ or less are neglected as their contribution to the solution is negligible. The orders under consideration are $O(r) = O(u) = O(v) = 1, O(z) = O(w) = \delta, O(N) = \frac{1}{\delta}, O\left(\frac{\mu_{nf}}{\rho_{nf}}\right) = O\left(\frac{\varkappa}{\rho_{nf}}\right) = O(j) = \delta^2$ where δ is the boundary layer thickness.[24] Under these assumptions and on neglecting external forces (body forces/body couples) and viscous dissipation term, our equations become

$$\frac{\partial w}{\partial z} + \frac{u}{r} + \frac{\partial u}{\partial r} = 0, \tag{8}$$

$$u\frac{\partial u}{\partial r} - \frac{v^2}{r} + w\frac{\partial u}{\partial z} = \frac{\varkappa}{\rho_{nf}}\left(\frac{\partial N}{\partial z}\right) + \left(\frac{\mu_{nf} + \varkappa}{\rho_{nf}}\right)\left(\frac{\partial^2 u}{\partial z^2}\right), \tag{9}$$

$$\frac{uv}{r} + u\frac{\partial v}{\partial r} + w\frac{\partial v}{\partial z} = \left(\frac{\mu_{nf} + \varkappa}{\rho_{nf}}\right)\left(\frac{\partial^2 v}{\partial z^2}\right), \tag{10}$$

$$u\frac{\partial N}{\partial r} + w\frac{\partial N}{\partial z} = -\frac{\varkappa}{\rho_{nf} j}\left(2N + \frac{\partial u}{\partial z}\right) + \left(\frac{\gamma_{nf}}{\rho_{nf} j}\right)\left(\frac{\partial^2 N}{\partial z^2}\right), \tag{11}$$

$$w\frac{\partial T}{\partial z} + u\frac{\partial T}{\partial r} = \alpha_{nf}\left(\frac{\partial^2 T}{\partial z^2}\right), \tag{12}$$

and the boundary conditions are

$$u|_{z=0} = U_w = rm\sin\varphi, v|_{z=0} = V_w = r\Omega\sin\varphi, w|_{z=0} = 0, N|_{z=0} = -n\frac{\partial u}{\partial z}, T|_{z=0} = T_w\, u|_{z=\infty} = 0, v|_{z=\infty} = 0, N|_{z=\infty} = 0, T|_{z=\infty} = T_\infty, \tag{13}$$

where, U_w and V_w represent wall velocities, T_w and T_∞ are the wall and free stream temperatures ($T_w > T_\infty$), m is the stretching or shrinking rate where for stretching ($m > 0$) and for shrinking ($m < 0$). The value of w at infinity is not specified as it adjusts its value such that the continuity equation is satisfied. The boundary condition on N represents that the micro-rotation vector is directly related to shear stress with micro-gyration parameter (boundary parameter) n whose values vary between 0 and 1 that is, $0 \leq n \leq 1$ and which physically represents the rotational degree of freedom of micro-elements close to the wall surface. An increase in microgyration parameter enhances the flow.[15,39,41]

- The condition when $n = 0, N = 0$ represents zero spin condition, which physically means that the concentration of the micro-elements at the boundary is so strong that the particles close to the surface of the wall are unable to rotate relative to the surface.[15,26]
- The condition when $n = 0.5, N = -\frac{1}{2}\frac{\partial u}{\partial z}$ represents the fact that the anti-symmetric fragment of the stress tensor diminishes at the surface and depicts weak concentration of micro-elements.[15,25,26]
- The condition when $n = 1, N = -\frac{\partial u}{\partial z}$ is used in the formulation of turbulent boundary layer flows,[15,27] which is not of our concern.

The effective models, which are employed to study the fluid flow and heat transfer in two-component mixtures are[15,16,19]

$$\frac{\mu_{nf}}{\mu_f} = (1-\phi)^{-\frac{25}{10}},\ \frac{\rho_{nf}}{\rho_f} = (1-\phi) + \phi\left(\frac{\rho_p}{\rho_f}\right), \alpha_{nf} = \frac{k_{nf}}{(\rho C_p)_{nf}},\ \frac{(\rho C_p)_{nf}}{(\rho C_p)_f} = (1-\phi) + \phi\left(\frac{(\rho C_p)_p}{(\rho C_p)_f}\right),\ \frac{k_{nf}}{k_f} = \frac{2\phi(k_p - k_f) + (2k_f + k_p)}{(k_p + 2k_f) - \phi(k_p - k_f)}, \tag{14}$$

where ϕ denotes the concentration of nanoparticles ranging from $0 \le \phi \le 0.2$. α_{nf} is the thermal diffusivity. The symbols $\rho_p, k_p, (\rho C_p)_p$ and $\rho_f, k_f, (\rho C_p)_f$ represent density, thermal conductivity, heat capacitance of solid nanoparticles, and base fluid, respectively. The subscripts f, nf, and p symbolize thermophysical properties of base fluid, nanofluid and solid nanoparticles in nanofluid, respectively. We also assume a gyro viscosity coefficient γ_{nf} (also known as spin gradient viscosity) relation as a variable depending upon nanofluid dynamic viscosity $\gamma_{nf} = (\mu_{nf} + 0.5\varkappa)\, j$.[15,25,33,35] This condition shows that in the limiting case, micro-structure effects near the solid boundary become negligible, and the rotation is only due to fluid shear, and therefore angular velocity and gyration vector becomes identical.[15,41] We also assume micro-inertia density relation to be $j = \frac{\nu_f}{|m|\sin\varphi}$, inversely depending on the stretching/shrinking rate and cone half-angle.[25,41] To transform boundary layer partial differential equations to ordinary differential equations, we make use of similarity transformations with η as a similarity variable[1]:

$$u = r|m|\sin\varphi F(\eta),\ v = r|m|\sin\varphi G(\eta),\ w = \left(\nu_f |m| \sin\varphi\right)^{\frac{1}{2}} H(\eta)\ T = T_\infty + \theta(\eta)\,(T_w - T_\infty), \tag{15}$$
$$N = r|m|\sin\varphi\left(\frac{|m|\sin\varphi}{\nu_f}\right)^{\frac{1}{2}} M(\eta), \eta = z\left(\frac{|m|\sin\varphi}{\nu_f}\right)^{\frac{1}{2}}.$$

The transformed boundary layer expressions of law of conservation of mass, linear momentum, angular-momentum, energy, and the corresponding boundary conditions using Equations 14 and 15, in the dimensionless form are written as

$$2F + H' = 0, \tag{16}$$

$$\frac{\left((1-\phi)^{-\frac{25}{10}} + \Delta\right)}{(1-\phi) + \phi\left(\frac{\rho_p}{\rho_f}\right)} F'' + \frac{\Delta}{(1-\phi) + \phi\left(\frac{\rho_p}{\rho_f}\right)} M' - HF' - F^2 + G^2 = 0, \tag{17}$$

$$\frac{\left((1-\phi)^{-\frac{25}{10}} + \Delta\right)}{(1-\phi) + \phi\left(\frac{\rho_p}{\rho_f}\right)} G'' - HG' - 2FG = 0, \tag{18}$$

$$\frac{\left((1-\phi)^{-\frac{25}{10}} + \frac{\Delta}{2}\right)}{(1-\phi) + \phi\left(\frac{\rho_p}{\rho_f}\right)} M'' - \frac{\Delta}{(1-\phi) + \phi\left(\frac{\rho_p}{\rho_f}\right)} (2M + F') - HM' - FM = 0, \tag{19}$$

$$\frac{\left(\frac{k_{nf}}{k_f}\right)}{\phi\left(\frac{\left(\rho C_p\right)_p}{\left(\rho C_p\right)_f}\right)+(1-\phi)}\theta''-\mathrm{Pr}H\theta'=0, \tag{20}$$

$$F(0)=d,G(0)=\omega,H(0)=0,M(0)=-nF'^{(0)},\theta(0)=1\ F(\infty)=0,G(\infty)=0,M(\infty)=0,\theta(\infty)=0, \tag{21}$$

where $\Delta=\frac{\varkappa}{\mu_f}$ is known as a micropolar parameter, $\omega=\frac{\Omega(\text{rotation})}{|m|(\text{deforandmationrate})}$ is rotation parameter, $\mathrm{Pr}=\frac{\nu_f}{\alpha_f}$ is Prandtl number, $d=\ \pm 1$ represents stretching ($d=1$) or shrinking parameter ($d=\ -1$). Equations 16–21 reduce to non-dimensional boundary layer equations for Newtonian viscous fluid if $\phi=\varkappa=n=0$,[1] and the micro-structure effects of the fluid do not significantly affect the velocity and temperature fields. When the fluid comes in contact with the surface of the deformable rotating heated cone, the role of skin friction along the meridional (tangential) r and azimuthal (circumferential) θ directions and also the heat transfer rate cannot be ignored. Therefore, the relevant physical parameters of our concern can be calculated by the following relations.[16,40,41]

$$C_{f_r}=\frac{\tau_r^*}{\rho_f U_w^2},\ C_{f_\theta}=\frac{\tau_\theta^*}{\rho_f U_w^2},\ Nu=\frac{qr}{(T_w-T_\infty)\,k_f}, \tag{22}$$

where the stretching shear stress, rotational shear stress, and heat flux can be calculated by

$$\tau_r^*=\left(\mu_{nf}+\varkappa\right)\frac{\partial u}{\partial z}+\varkappa N\Big|_{z=0},\tau_\theta^*=\left(\mu_{nf}+\varkappa\right)\frac{\partial v}{\partial z}\Big|_{z=0},q=-k_{nf}\frac{\partial T}{\partial z}\Big|_{z=0}, \tag{23}$$

which after simplification takes the form

$$C_{f_r}=\left[(1-\phi)^{-\frac{25}{10}}+(1-n)\,\Delta\right]\sqrt{\frac{\nu_f}{r^2 m\sin\varphi}}F'^{(0)}C_{f_r}\mathrm{Re}^{\frac{1}{2}}=\left[(1-\phi)^{-\frac{25}{10}}+(1-n)\,\Delta\right]F'^{(0)}, \tag{24}$$

$$C_{f_\theta}=\left[(1-\phi)^{-\frac{25}{10}}+\Delta\right]\sqrt{\frac{\nu_f}{r^2 m\sin\varphi}}G'^{(0)}C_{f_\theta}\mathrm{Re}^{\frac{1}{2}}=\left[(1-\phi)^{-\frac{25}{10}}+\Delta\right]G'^{(0)}, \tag{25}$$

$$Nu=-\frac{k_{nf}}{k_f}\sqrt{\frac{r^2 m\sin\varphi}{\nu_f}}\theta'^{(0)}Nu\mathrm{Re}^{-\frac{1}{2}}=-\frac{k_{nf}}{k_f}\theta'^{(0)}, \tag{26}$$

where the local Reynolds number is

$$\mathrm{Re}=\frac{r^2 m\sin\varphi}{\nu_f}.$$

3 | SOLUTION METHODOLOGY

Equations 16–20 corresponding to the boundary conditions represented by Equation 21 are solved by bvp4c, which is a numerical technique. It requires an initial guess to solve boundary value problems. In this method, the system of second-order differential equations is first converted into the first-order differential equation, then the appropriate initial guess is selected, which satisfies the boundary conditions so as to obtain the desired solution. In the current study, the effects of the concerned parameters on velocity, temperature, micro-rotation fields, and on skin friction and Nusselt number are analyzed from the solution obtained by this method.

4 | DISCUSSION OF NUMERICAL RESULTS

This section is concerned with the graphical and numerical discussion of the effect of various embedding parameters such as rotation parameter ω, nanoparticles concentration parameter ϕ, and micropolar parameter Δ on velocity, temperature, and micro-rotation fields. The impact on skin friction coefficients and Nusselt number for these emerging parameters are also presented in Tables 3–5. The whole analysis is carried out considering stretching as well as the shrinking of the cone surface in both cases of weak and strong concentration of micro-elements. The thermophysical properties of the concerned constituents are given in Table 1.[13,16,40]

To check the validation of the present results, we first compare these results with the previous publications considering $\Delta = n = \phi = 0$. After non-dimensionalizing Equation 23 and substituting it in Equation 22, if we simplify skin friction coefficients and Nusselt number in a different manner likewise in the work of Turkyilmazoglu,[1] we get

$$C_{f_r} = \left[(1-\phi)^{-\frac{25}{10}} + (1-n)\,\Delta\right]\sqrt{\frac{\nu_f}{r^2 m \sin^4\varphi}}(\sin\varphi)^{\frac{3}{2}}F'(0)\; C_1 = \left[(1-\phi)^{-\frac{25}{10}} + (1-n)\,\Delta\right](\sin\varphi)^{\frac{3}{2}}F'(0). \tag{27}$$

$$C_{f_\theta} = \left[(1-\phi)^{-\frac{25}{10}} + \Delta\right]\sqrt{\frac{\nu_f}{r^2 m \sin^4\varphi}}(\sin\varphi)^{\frac{3}{2}}G'^{(0)} C_2 = \left[(1-\phi)^{-\frac{25}{10}} + \Delta\right](\sin\varphi)^{\frac{3}{2}}G'^{(0)}. \tag{28}$$

$$Nu = -\frac{k_{nf}}{k_f}\sqrt{\frac{r^2 m}{\nu_f}}(\sin\varphi)^{\frac{1}{2}}\theta'^{(0)} = -\frac{k_{nf}}{k_f}(\sin\varphi)^{\frac{1}{2}}\theta'^{(0)}. \tag{29}$$

As it is clear from Table 2, the results obtained are in good agreement with the previous results, so we can assume that our results are correct, and therefore, we can analyze the influence of various emerging parameters on a

TABLE 1 Thermo-physical properties of *water* ($Pr = 6.2$),Cu,Al_2O_3,TiO_2.

Properties/Constituents	Water	Cu	Al_2O_3	TiO_2
ρ (kg/m^3)	997.1	8933.0	3970.0	4250.0
k (W/K. m)	0.6130	401.0	40.0	8.9538
C_p (J/kg. K)	4179.0	385.0	765.0	686.2

TABLE 2 Comparison of the values of skin friction coefficients and Nusselt number when $\Delta = n = \phi = 0$ (viscous fluid) for stretching ($d = +1$) as well as for shrinking ($d = -1$) rotating cone case for variation of cone apex half angle using Equations 27–29

Parameter		C_1		C_2		C_3	
ω	ϕ	[1]	Present	[1]	Present	[1]	Present
$d = 1$							
5	90	3.19374	3.19374	−9.25353	−9.25353	1.12914	1.12914
	70	2.90923	2.90923	−8.42919	−8.42919	1.09456	1.09456
	50	2.14131	2.14131	−6.20423	−6.20423	0.98826	0.98826
	30	1.12916	1.12916	−3.27162	−3.27162	0.79842	0.79842
	10	0.23110	0.23110	−0.66959	−0.66959	0.47052	0.47052
$d = -1$							
5	90	7.82333	7.82333	−4.25913	−4.25912	0.64626	0.64626
	70	7.12641	7.12641	−3.87971	−3.87971	0.62647	0.62647
	50	5.24533	5.24533	−2.85563	−2.85562	0.56563	0.56563
	30	2.76597	2.76597	−1.50583	−1.50583	0.45697	0.45697
	10	0.56610	0.56610	−0.30819	−0.30819	0.26930	0.26930

deformable rotating cone model in micropolar nanofluid. Figures 2 and 3 illustrate the effect of rotation parameter on velocity, temperature, and micro-rotation fields for stretching/shrinking of a deformable rotating cone for Cu nanoparticles in water. Solid lines represent a strong concentration (zero spin condition) of micro-elements when $n = 0$, and dashed lines represent a weak concentration of micro-elements when $n = 0.5$ at the boundary. Figure 2A shows that as the rotation parameter $\omega = \frac{\Omega}{|m|}$ enhances, the rotation of the cone increases; as a result centrifugal forces come into play. This centrifugal force compels the fluid to move away from the surface of the cone (in an outward direction), but the effect of this force only remains prominent in the vicinity of the cone surface. Thus, the dimensionless tangential F-component of the velocity increases rapidly by an increase in ω only in the vicinity of the cone surface and

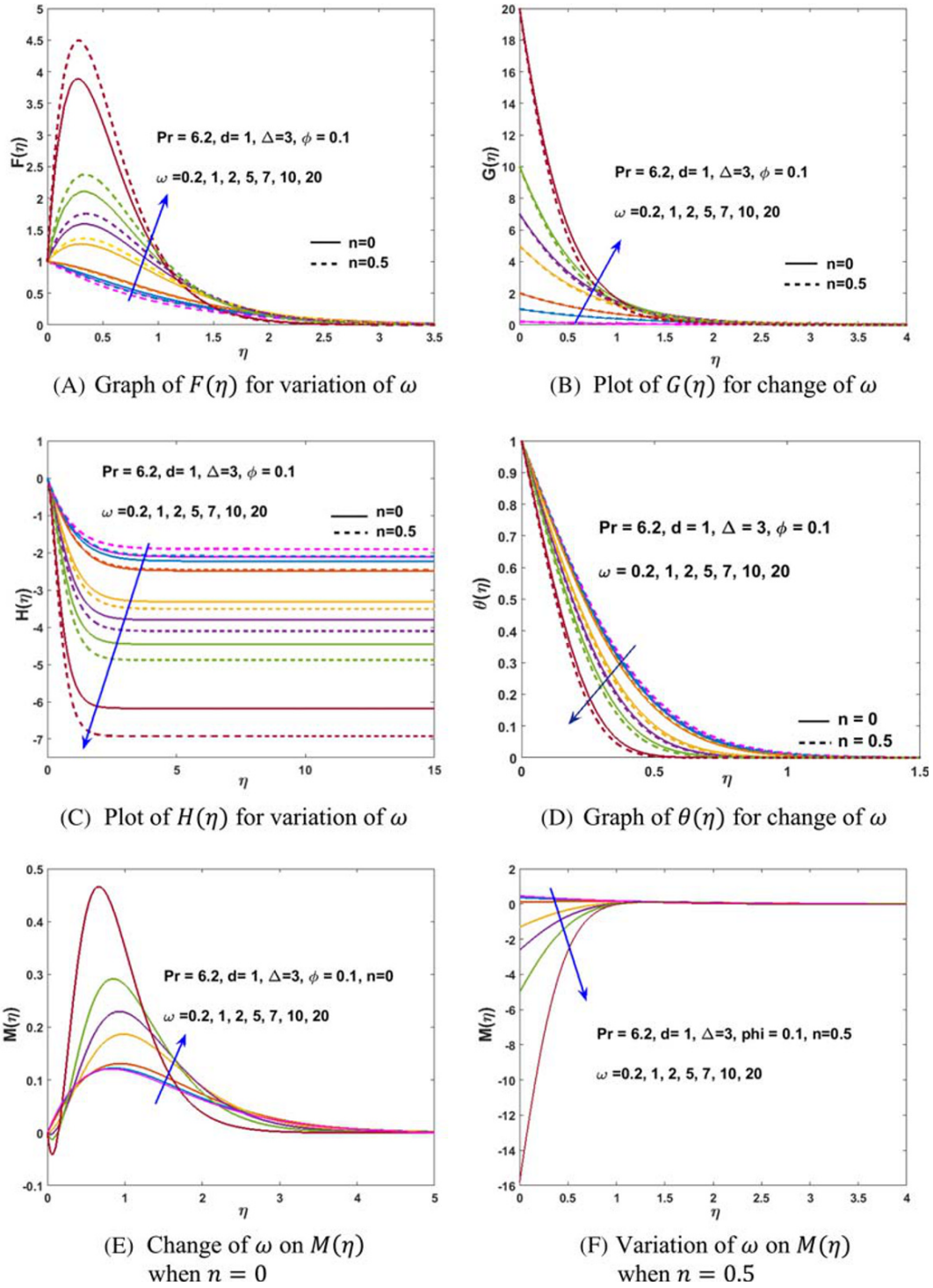

FIGURE 2 Impact of cone rotation parameter ω on the boundary layer [Colour figure can be viewed at wileyonlinelibrary.com]

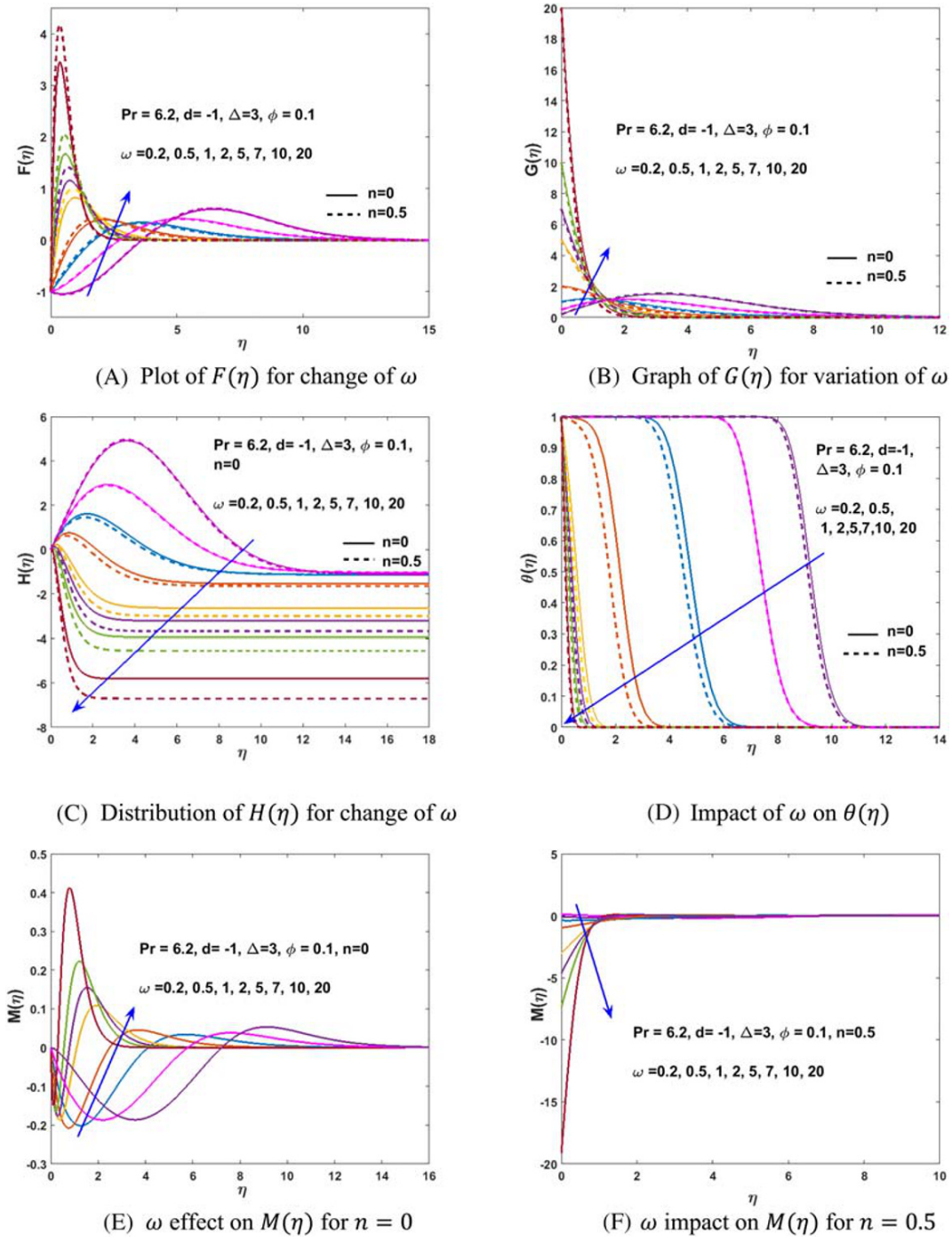

FIGURE 3 Impact of cone rotation parameter ω on the boundary layer at various values of n [Colour figure can be viewed at wileyonlinelibrary.com]

diminishes away from the surface. A large value of the rotation parameter indicates that the rotation is greater than the stretching rate of the cone surface. The graph further depicts the behavior of tangential F-component of the velocity profile in case of a weak and strong concentration of micro-elements. For weak concentration, the velocity is high for large values of ω ($\Omega > |m|$) and is slightly low for small values of ω ($|m| > \Omega$). When the stretching is more prominent than the rotation, the flow is greatly affected by the stretching than the rotation, so for weak concentration, the velocity decreases. Figure 2B illustrates that the dimensionless azimuthal G-component of the velocity increases as the rotation increases and is nearly the same for both strong and weak concentrations of micro-elements for small values of ω; however, it is slightly less for weak concentration as compared to the strong concentration of micro-elements for large values of ω. Figure 2C depicts that the dimensionless normal H-component of the velocity increases in the negative

direction with the growth of rotation parameter (showing inward flow); the reason is that the centrifugal force compels the fluid to move in outward direction; thus, in order to balance it, fluid away from the surface tends to move towards the surface of the cone causing inward flow, and this inward flow increases as ω increases, due to which continuity equation is satisfied. Like the F-component of velocity, for a weak concentration of micro-elements, the increase in the negative direction is more for large values of rotation parameter whereas for the case when the stretching rate is greater than rotation, the velocity decreases as compared to that for strong concentration. Figure 2D shows that the temperature distribution declines as ω enhances due to reduction in stretching rate and this decline in temperature for strong and weak concentration is different for various rotation parameters that is, for small rotation parameters, the decline in temperature profile is more for strong concentration and for large rotation parameters the decline in temperature profile is more for weak concentration of micro-elements. Figure 2E illustrates that the micro-rotation profile for the case of zero spin condition is zero (micro-elements are unable to rotate) at the surface of the boundary, and it increases with the increase in rotation parameter, and far away from the surface, it diminishes away. Figure 2F shows that the micro-rotation profile, for a weak concentration of micro-elements, increases in the negative direction as the rotation parameter increases due to the boundary condition. In the case of shrinking and rotating cone surface, the phenomena of reverse flow occur, which is absent in stretching and rotating cone surface. Moreover Figure 3A–D illustrates that at high values of rotation parameter, shrinking and rotating cone behavior is similar to stretching and rotating cone behavior. Figure 3A represents that at low values of rotation parameter (for $\omega < 1$) shrinking is more dominant than rotation due to which inward flow occurs. High values of rotation parameter show the rotations are more dominant than shrinking due to which centrifugal force comes into existence, which forces the fluid in an outward direction and so the dimensionless tangential F-component of velocity increases rapidly as ω increases. The weak concentration of micro-elements shows higher velocity profile then strong concentration for high rotation parameters. Figure 3B displays the dimensionless azimuthal G-component of velocity increases as rotation parameter increases, and weak concentration of micro-elements shows slightly less velocity profile for high rotation parameters like in stretching case. Figure 3C portrays that outward flow occurs for small rotation parameters and inward flow occurs for large rotation parameters, thus satisfying the law of conservation of mass. For a weak concentration of micro-elements, inward flow is more than that for strong concentration at large rotation parameters. Figure 3(d) depicts the temperature distribution declines with the enlargement of the rotation parameter, and the decline in temperature distribution is more for weak concentrations. This behavior is due to a decrease in the shrinking rate. Figure 3E illustrates that the micro-rotation profile for strong concentrations at the surface is zero (micro-elements are unable to rotate) and grows in the vicinity of the surface with the growth of rotation parameter, but far away from the surface, it approaches to zero. From Figure 3F, it can be deduced that for weak concentrations, micro-rotation profile increases in the negative direction with the increase in the rotation parameter due to its boundary condition. From Figures 2 and 3, it can be deduced that the increase in rotation parameter causes a reduction in both momentum and thermal boundary layers. Figure 4A–C represents the fact that the increase in nanoparticle concentration hinders the fluid motion and causes a decrease in velocity for all three nanoparticles. It is observed that the most prominent decrease is for Cu – water whereas the base fluid has the highest velocity profile. Thus, increase in nanoparticle volume fraction parameter leads to a thinner momentum boundary layer. The difference in velocities of nanoparticles is due to the difference in their densities. Cu has a high density, so it offers more resistance. Figure 4D shows that an increase in nanoparticle concentration leads to heat generation. Cu – water shows the highest temperature, Al_2O_3 – water shows slightly less temperature than Cu – water, and TiO_2 – water shows the lowest temperature among the nanoparticles. The difference in temperature is due to the difference in the thermal conductivities of nanoparticles. An increase in the concentration of nanoparticles increases the temperature of the fluid, causing a decrease in the temperature gradient, but due to the significant enhancement in the thermal conductivity of the fluid, the rate of heat transfer increases. An increase in temperature leads to the thickening of the thermal boundary layer. For weak concentration, the behavior of velocity and temperature distribution for change in nanoparticles remains the same as for strong concentration. For a strong concentration of micro-elements (zero spin condition), Figure 4E shows a decline in the micro-rotation profile as nanoparticles concentration enhances. Figure 4F represents that the micro-rotation profile for a weak concentration of micro-elements has dual behavior for an increase in nanoparticle concentration. Near the surface, base fluid has the lowest profile whereas far away from the surface, base fluid has the highest profile, which shows that the effect of nanoparticles on micro-rotation is more prominent near the surface. It is clearly observed from Figure 4E,F that micro-rotation profile for strong concentration is low as compared to that for a weak concentration of micro-elements. It is illustrated in Figure 5A that an increase in nanoparticle concentration parameter decreases the inward flow (near the surface) as well as the outward flow (away from the surface). Thus, the velocity profile decreases, and the most prominent change is for Cu – water. From Figure 5B,C,

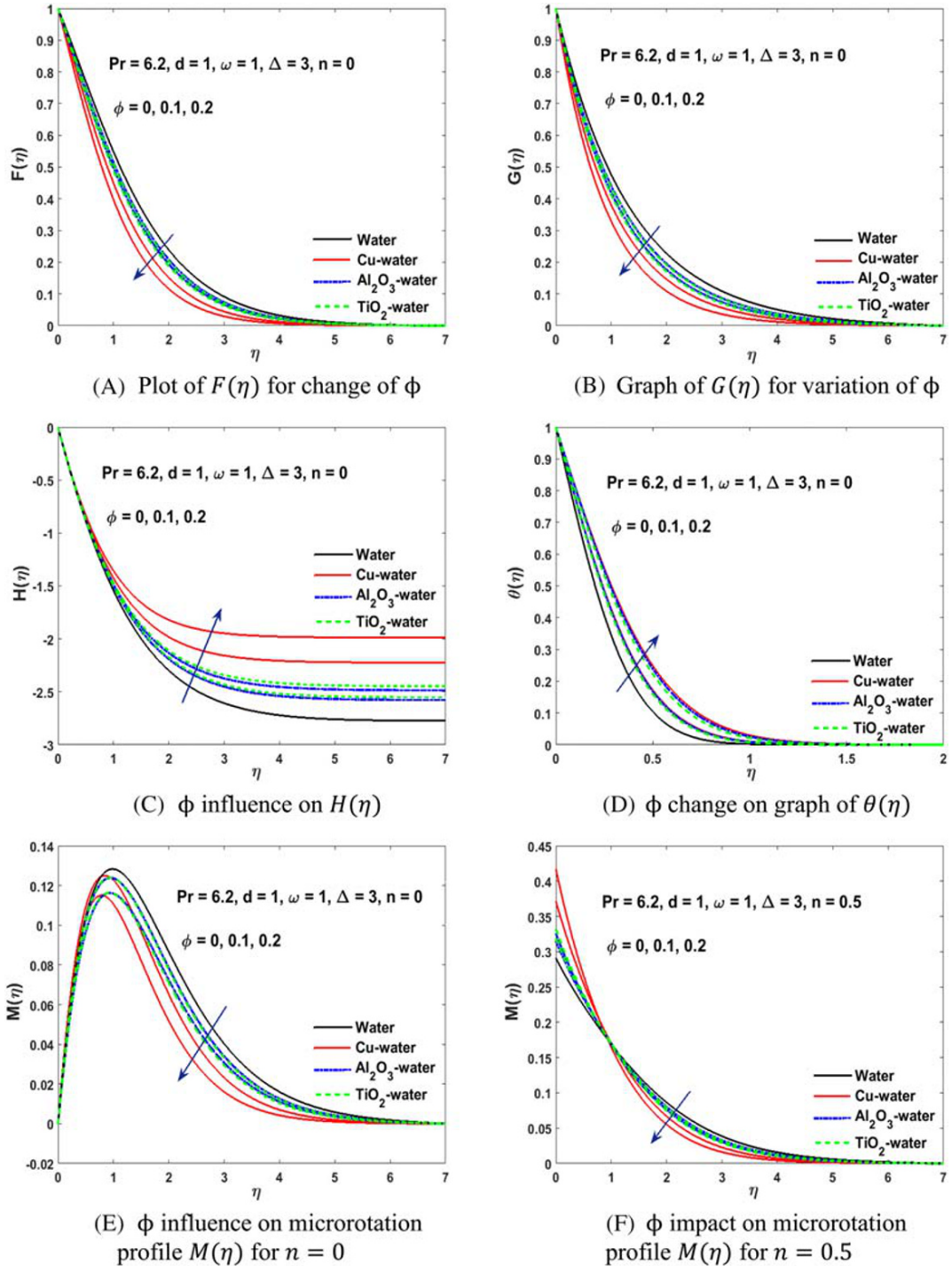

FIGURE 4 Impact of volume fraction of nanoparticles on the boundary layer of a stretching surface for various types of nanoparticles [Colour figure can be viewed at wileyonlinelibrary.com]

decreases in velocity profile for an increase in nanoparticle concentration are observed as resistance increases. Figure 5D depicts the behavior of temperature profile that it decreases as nanoparticles concentration increases, and the base fluid water has the highest temperature distribution. This behavior is due to the difference in their densities and specific heats. For both strong and weak concentrations of micro-elements, the behavior of velocity and temperature distribution for change in nanoparticles remains the same. Figure 5E,F shows fluctuating behavior for the raise in nanoparticle volume fraction for both strong and weak concentrations of micro-elements. Therefore, it can be deduced that in case of shrinking rotating cone, an increase in nanoparticle concentration decreases both momentum and thermal boundary layers. Figure 6A–C illustrates that the velocity profile increases as micropolar parameter increases,

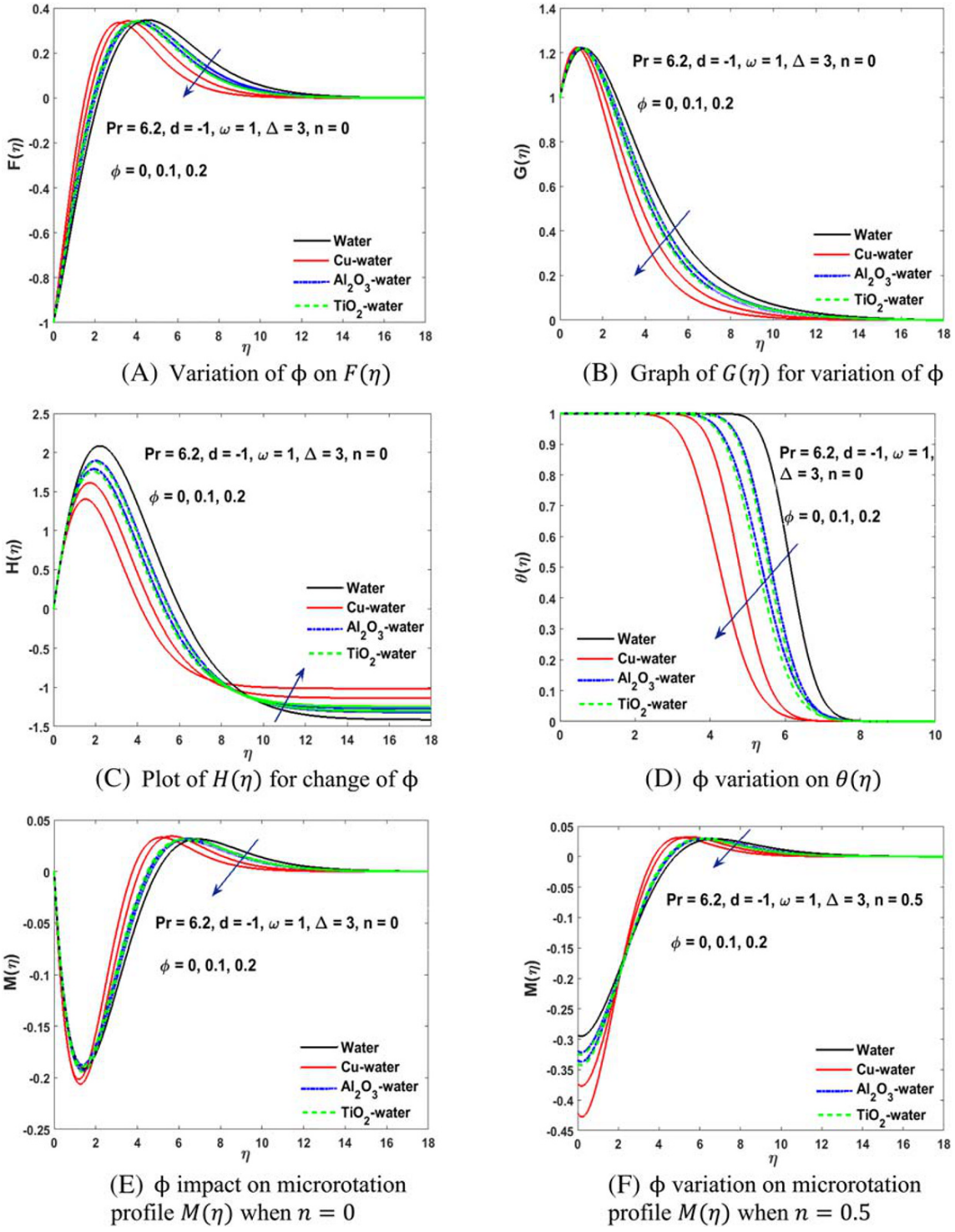

FIGURE 5 Impact of volume fraction of nanoparticles on the boundary layer of a shrinking surface for various types of nanoparticles [Colour figure can be viewed at wileyonlinelibrary.com]

which is the ratio of vortex viscosity to the dynamic viscosity. An increase in micropolar parameter increases the velocity of the fluid as vortex viscosity increases or the dynamic viscosity of the fluid decreases, which accelerates the fluid motion. Thus, an increase in micropolar parameter leads to a thicker momentum boundary layer. Figure 6C shows that the normal H-component of velocity increases in negative direction showing inward flow is maximum for Al_2O_3 – water and is minimum for Cu – water, just like the outward flow for Al_2O_3 – water is maximum and for Cu – water is minimum from Figure 6A. This behavior satisfies the law of conservation of mass. Figure 6D demonstrates that the increase

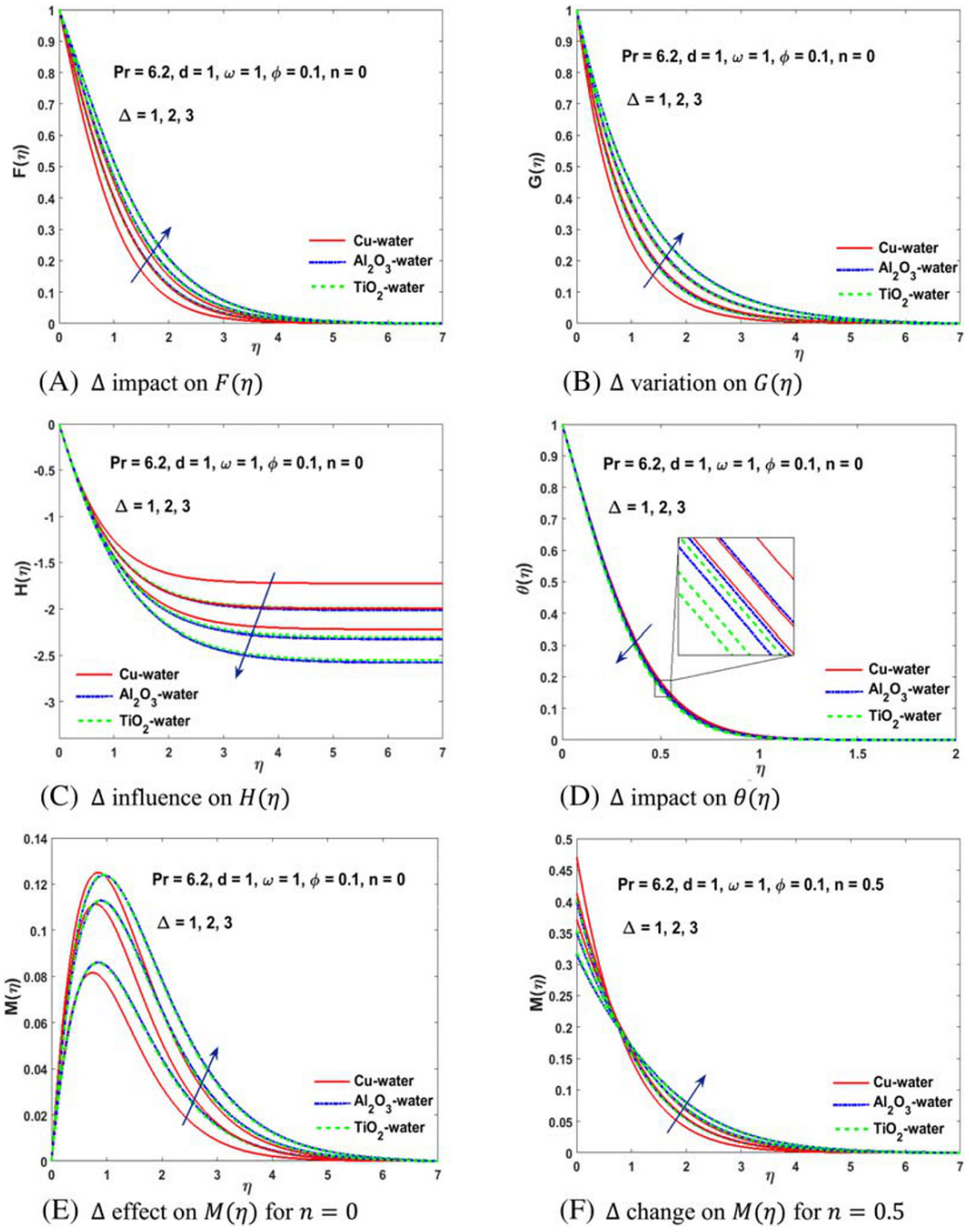

FIGURE 6 Impact of Δ on the boundary layer of a stretching surface for various types of nanoparticles [Colour figure can be viewed at wileyonlinelibrary.com]

in micropolar parameter decreases the temperature of the fluid and TiO_2 – water shows the minimum temperature whereas Cu – water shows maximum temperature profile; thus, enhancement in micropolar parameter leads to a thinner thermal boundary layer. The increase and decrease in velocity and temperature distributions are due to the difference in densities and thermal conductivities of nanoparticles. For a weak concentration of micro-elements, velocity and temperature distribution for change in micropolar parameter remains the same as for strong concentration. Figure 6E demonstrates that the micro-rotation profile increases as the micropolar parameter increases due to the increase in micropolar behavior. Figure 6F depicts the behavior that enhancement of micropolar parameter shows dual behavior for the micro-rotation profile. Near the surface, the micro-rotation profile decreases, whereas away from the surface, it increases. Figure 7A illustrates that the enhancement of micropolar parameter results in an increase in the inward flow (near the surface) and the outward flow (away from the surface); thus, the velocity profile increases. Figure 7B shows

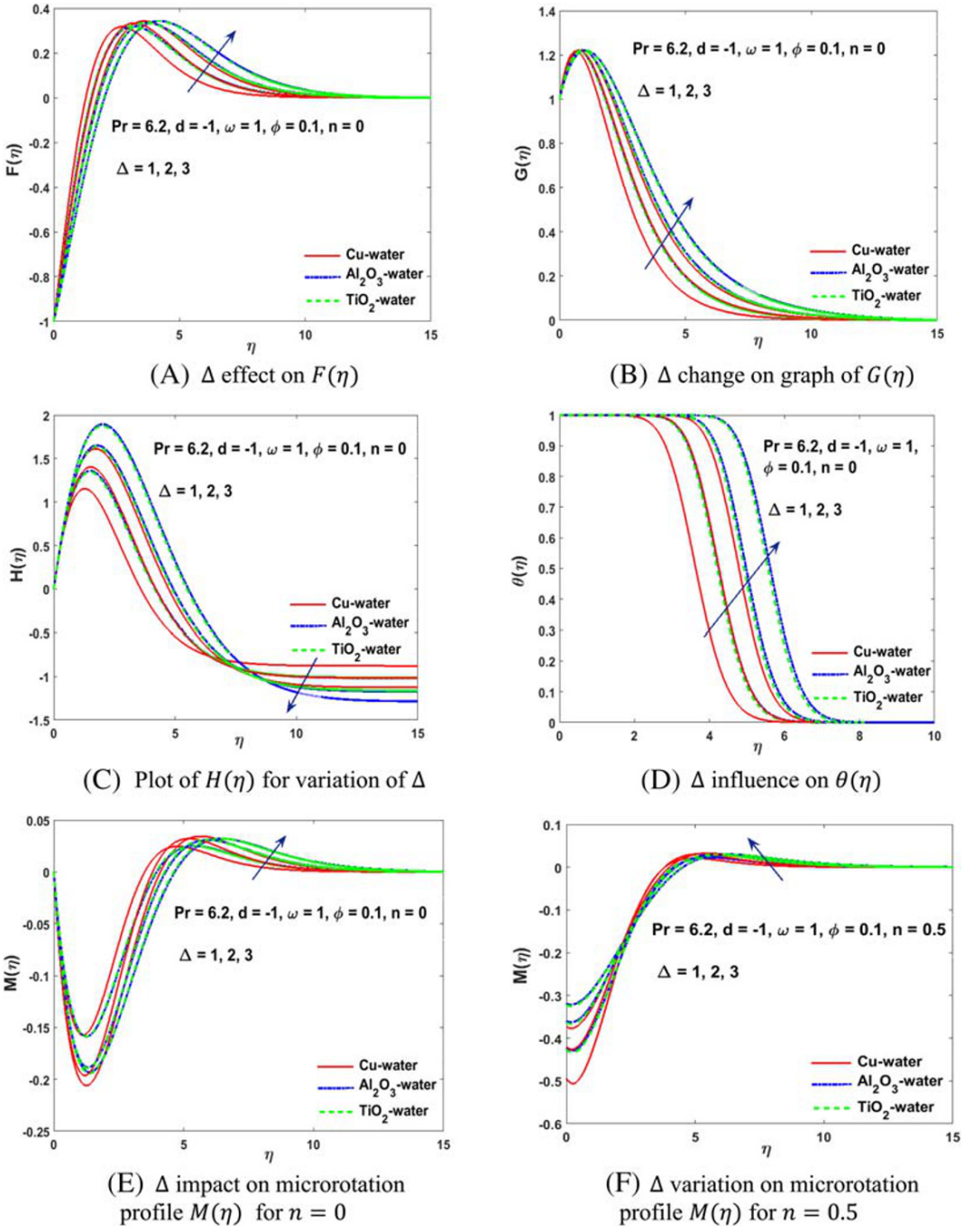

FIGURE 7 Impact of Δ on the boundary layer of a shrinking surface for various types of nanoparticles [Colour figure can be viewed at wileyonlinelibrary.com]

that the azimuthal G-component of velocity rises with the growth of micropolar parameter like in stretching case. Figure 7C depicts that the outward flow (close to the boundary) and the inward flow (away from the boundary) increases as Δ increases; thus, the normal H-component of the velocity increases in order to balance the continuity equation. From Figure 7A–C, it can be deduced that the increase in micropolar parameter thickens the momentum boundary layer. The temperature profile enhances with the increment of the micropolar parameter, which is shown in Figure 7D, thus leading to a thicker thermal boundary layer. Al_2O_3 – water shows the highest temperature whereas Cu – water shows the lowest temperature with an increase in Δ. Such behavior in velocity and temperature distributions is due to differences in densities and specific heats of nanoparticles, and it remains the same for a weak and strong concentration of micro-elements. Figure 7E illustrates that the micro-rotation profile becomes zero for all three

TABLE 3 Variation of ω on skin friction coefficients $C_{f_r}\mathrm{Re}^{\frac{1}{2}}, C_{f_\theta}\mathrm{Re}^{\frac{1}{2}}$ and Nusselt number $Nu\mathrm{Re}^{\frac{1}{2}}$ of Cu – water for stretching/shrinking rotating cone case with $Pr = 6.2$ using Equations 24–26

Parameter			$d = 1$		$d = -1$	
ω	Δ	ϕ	$n = 0$	$n = \frac{1}{2}$	$n = 0$	$n = \frac{1}{2}$
$C_{f_r}Re^{\frac{1}{2}}$						
1	3	0.1	−2.45312	−2.08083	2.57179	2.08901
2			−0.70433	−0.58722	6.72158	5.41120
3			1.90587	1.56775	11.20813	8.92964
5			9.11899	7.36987	21.39843	16.84004
$C_{f_\theta}Re^{\frac{1}{2}}$						
1	3	0.1	−4.09764	−3.98175	2.41008	2.04801
2			−8.65205	−8.60291	0.12041	−0.70474
3			−13.78519	−13.93821	−3.12768	−4.40914
5			−25.71258	−26.52868	−11.97454	−14.29197
$NuRe^{\frac{1}{2}}$						
1	3	0.1	2.99093	2.94282	0.00000	0.00000
2			3.07114	3.05343	0.00791	0.03399
3			3.18224	3.19778	0.19538	0.37534
5			3.44028	3.51175	0.89597	1.18757

TABLE 4 Influence of Δ and ϕ on skin friction coefficients $C_{f_r}\mathrm{Re}^{\frac{1}{2}}, C_{f_\theta}\mathrm{Re}^{\frac{1}{2}}$ and Nusselt number $Nu\mathrm{Re}^{\frac{1}{2}}$ for stretching rotating cone case ($d = 1$) with $Pr = 6.2$ using Equations 24–26

Parameter			Cu		Al O		TiO	
ω	Δ	ϕ	$n = 0$	$n = \frac{1}{2}$	$n = 0$	$n = \frac{1}{2}$	$n = 0$	$n = \frac{1}{2}$
$C_{f_r}\mathrm{Re}^{\frac{1}{2}}$								
3	3	0.0	1.43299	1.17962	1.43299	1.17962	1.43299	1.17962
		0.1	1.90587	1.56775	1.64905	1.36936	1.66494	1.38165
		0.2	2.33086	1.94465	1.87375	1.58081	1.90324	1.60427
3	0	0.1	0.92823	0.92823	0.78918	0.78918	0.79767	0.79767
	1		1.28124	1.13070	1.09928	0.97321	1.11040	0.98283
	3		1.90587	1.56775	1.64905	1.36936	1.66494	1.38165
$C_{f_\theta}\mathrm{Re}^{\frac{1}{2}}$								
3	3	0.0	−9.91038	−10.03085	−9.91038	−10.03085	−9.91038	−10.03085
		0.1	−13.78519	−13.93822	−11.71607	−11.84563	−11.84234	−11.97336
		0.2	−17.40965	−17.57919	−13.65636	−13.78911	−13.89495	−14.03009
3	0	0.1	−7.60044	−7.60044	−6.46191	−6.46191	−6.53143	−6.53143
	1		−10.10145	−10.16378	−8.58681	−8.63987	−8.67929	−8.73292
	3		−13.78519	−13.93822	−11.71607	−11.84563	−11.84234	−11.97338
$Nu\mathrm{Re}^{\frac{1}{2}}$								
3	3	0.0	2.78582	2.79258	2.78582	2.79258	2.78582	2.79258
		0.1	3.18224	3.19778	3.14355	3.15398	3.08216	3.09260
		0.2	3.58063	3.60109	3.50975	3.52245	3.37922	3.39169
3	0	0.1	3.11508	3.11508	3.11469	3.11469	3.05354	3.05354
	1		3.16528	3.17726	3.14293	3.15264	3.08121	3.09075
	3		3.18224	3.19778	3.14355	3.15399	3.08216	3.09260

nanoparticles when micropolar effects are neglected in case of strong concentration (no spin condition) of micro-elements. A decrease in micro-rotation near the surface but an increase when away from the surface is observed when the micropolar parameter is enhanced. Figure 7F shows an increase in micro-rotation as micropolar effects are increased for a weak concentration of micro-elements. The physically important quantities of our interest for practical application are skin friction coefficients and Nusselt numbers, which are calculated by the relations given in Equations 24–26. By using Equations 27–29, we can calculate skin friction coefficients and Nusselt number for different cone half angles. Numerically calculated data for skin friction coefficients and Nusselt number are represented in tables for variation in rotation parameter, nanoparticle concentration parameter, and micropolar parameter for strong and weak concentrations when rotating cone wall is subjected to stretching as well as shrinking. Growth of rotation parameter in micropolar nanofluid results in an increment in skin friction as well as in Nusselt number. The reason is that an increase in rotation causes a collision of nanoparticles, which increases friction between fluid and nanoparticles. Moreover, these collisions boost the rate of heat transfer in both cases for strong/weak concentrations of stretching/shrinking of the rotating cone. Skin friction as well as Nusselt number both increase for all nanoparticles when nanoparticle concentration parameter is increased. Addition of nanoparticles results in thickening of fluid as well as increase in its thermal conductivity due to which local skin friction and the heat transfer rate increases. This behavior is observed in both cases when rotating cone is subjected to stretching or shrinking for strong as well as weak concentrations of micro-elements. In case of stretching rotating cone, enhancement in micropolar parameter results in a rise in skin friction and Nusselt number. In contrast, in case of shrinking rotating cone, skin friction rises, and Nusselt number declines as micropolar parameter increases; this behavior is observed for all nanoparticles in the presence of strong/weak concentration of micro-elements. In all the above cases, Cu – water shows maximum skin friction and Nusselt number, Al_2O_3 – water shows minimum skin friction and TiO_2 – water shows minimum Nusselt number. This behavior is due to a difference

TABLE 5 Influence of Δ and ϕ on skin friction coefficients $C_{f_r}\mathrm{Re}^{\frac{1}{2}}, C_{f_\theta}\mathrm{Re}^{\frac{1}{2}}$ and Nusselt number $Nu\mathrm{Re}^{\frac{1}{2}}$ for shrinking rotating cone case ($d = -1$) with $Pr = 6.2$ using Equations 24–26

Parameter			Cu		Al O		TiO	
ω	Δ	ϕ	$n = 0$	$n = \frac{1}{2}$	$n = 0$	$n = \frac{1}{2}$	$n = 0$	$n = \frac{1}{2}$
$C_{f_r}\mathrm{Re}^{\frac{1}{2}}$								
3	3	0.0	7.88452	6.38398	7.88452	6.38398	7.88452	6.38398
		0.1	11.2081	8.92962	9.44396	7.66323	9.55152	7.74093
		0.2	14.32294	11.50032	11.12307	9.13745	11.3264	9.28852
3	0	0.1	6.40418	6.40418	5.44485	5.44485	5.50343	5.50343
	1		8.44306	7.18023	7.15841	6.13306	7.23689	6.19705
	3		11.20808	8.92962	9.44396	7.66323	9.55152	7.74093
$C_{f_\theta}\mathrm{Re}^{\frac{1}{2}}$								
3	3	0.0	−2.30449	−3.29841	−2.30449	−3.29841	−2.30449	−3.29841
		0.1	−3.12767	−4.40915	−2.68377	−3.76948	−2.71081	−3.80872
		0.2	−3.90448	−5.33524	−3.09391	−4.22217	−3.14529	−4.29340
3	0	0.1	−1.67079	−1.67079	−1.42052	−1.42051	−1.43579	−1.43579
	1		−2.23483	−2.75843	−1.90370	−2.35539	−1.92390	−2.38005
	3		−3.12767	−4.40915	−2.68377	−3.76948	−2.71081	−3.80873
$Nu\mathrm{Re}^{\frac{1}{2}}$								
3	3	0.0	0.01952	0.08264	0.01952	0.08264	0.01952	0.08264
		0.1	0.19230	0.36742	0.09785	0.22839	0.09293	0.21958
		0.2	0.45222	0.67372	0.23695	0.40675	0.21623	0.37735
3	0	0.1	0.67466	0.67466	0.52662	0.52662	0.51032	0.51032
	1		0.42772	0.53248	0.28784	0.39467	0.27728	0.38103
	3		0.18451	0.36742	0.08701	0.22839	0.08307	0.21958

in densities, and thermal conductivities of the nanoparticles as Cu nanoparticles have the maximum thermal conductivity and density, Al_2O_3 has minimum density, and TiO_2 has the minimum thermal conductivity.

The results of skin friction coefficients and Nusselt number are presented in the Tables 3–5.

5 | CONCLUDING REMARKS

This investigation explores the effect of rotation parameter, nanoparticle concentration parameter, and micropolar parameter for stretching/shrinking rotating cone in micropolar nanofluid in detail. Under the graphical and numerical results presented in Section 4, the following conclusions can be made:

- Growth of rotation parameter results in the thinning of both momentum as well as the thermal boundary layer. Moreover, skin friction, along with Nusselt number increases for strong/weak concentrations of stretching/shrinking rotating cone.
- An increase in nanoparticle concentration parameter leads to thinner momentum boundary layer and thicker thermal boundary layer for stretching rotating cone, whereas for shrinking rotating cone, both boundary layers thickness decreases. Skin friction as well as Nusselt number increases for enhancement in nanoparticles volume fraction parameter for strong as well as weak concentrations of stretching/shrinking rotating cone.
- For stretching rotating cone, enhancement in micropolar parameter leads to thicker momentum boundary layer and thinner thermal boundary layer. Skin friction as well as Nusselt number increases for a rise in micropolar parameter for both strong as well as weak concentrations of micro-elements.
- For a shrinking rotating cone, an increase in micropolar parameter leads to the growth of the momentum boundary layer as well as the thermal boundary layer, and skin friction increases, but Nusselt number decreases for strong/weak concentration of micro-elements.
- In all the above cases Cu – water displays the highest skin friction and Nusselt number, Al_2O_3 – water shows the lowest skin friction, and TiO_2 – water shows the lowest Nusselt number.
- An increase in skin friction physically means that more torque is required for steady rotation of the cone and the enhancement of Nusselt number leads to the cooling of the system.

CONFLICTS OF INTEREST

This work does not have any conflicts of interest.

NOMENCLATURE

Latin letters

u,v,w	velocity components, m/s
k	thermal conductivity
P	pressure, kg/ms^2
n	micro-gyration parameter (1)
q,T	heat flux and temperature respectively
M	dimensionless micro-rotation component (1)
Re	Reynolds number (1)
m_{st}	couple stress tensor
j	micro-inertia density per unit mass, m^2
F,G,H	dimensionless velocity components (1)
r,z	coordinate system (1)
N	micro-rotation vector
Nu	Nusselt number (1)
f	body forces
l	body couples per unit mass
Pr	Prandtl number (1)
t_{st}	stress tensor
ρc_p	heat capacitance

Greek letters

ζ	bulk viscosity
Ω	angular frequency, Rad/s
φ	cone half-angle (apex)
μ	dynamic viscosity, kg/ms
ν	kinematic viscosity, m^2/s
ρ	density, kg/m^3
α	thermal diffusivity, m^2/s
θ	dimensionless temperature (1)
C_{f_r}, C_{f_θ}	skin frictions in r and θ directions
τ_r^*, τ_θ^*	wall shear stresses along r and θ directions
$\varkappa$	vortex viscosity, kg/ms
χ,β,γ	gyro viscosity coefficients, kgm/s
$,\pi_v$	micro-rotation vector,1/s
$\varepsilon,\varepsilon_{tsv}$	alternating tensor of Levi-Civita.
Δ	micropolar parameter (1)
ω	dimensionless rotation parameter (1)
η	dimensionless similarity variable (1)
Φ	dissipation function (1)
ϕ	nanoparticles concentration parameter (1)

Subscripts

nf	nanofluid
f	fluid
p	solid nanoparticles
w,∞	denote wall and ambient conditions

ORCID

Anber Saleem https://orcid.org/0000-0002-7388-3946
Sohail Nadeem https://orcid.org/0000-0002-1052-011X
Mehdi Ghalambaz https://orcid.org/0000-0001-8762-5510

REFERENCES

1. Turkyilmazoglu M. A note on induced flow and heat transfer due to a deforming cone rotating in a quiescent fluid. *J Heat Transfer*. 2018;140(12):124502.
2. Tien CL. Heat transfer by laminar flow from a rotating cone. *J Heat Transf Trans ASME Ser C*. 1960;82:252-253.
3. Tien CL, Tsuji IJ. A theoretical analysis of laminar forced flow and heat transfer about a rotating cone. *J Heat Transf Trans ASME*. 1965; 87(2):184-190.
4. Hering RG, Grosh RJ. Laminar combined convection from a rotating cone. *ASME J Heat Transf*. 1963;85(1):29-34.
5. Takhar HS, Chamkha AJ, Nath G. Unsteady mixed convection flow from a rotating vertical cone with a magnetic field. *Heat Mass Transf*. 2003;39(4):297-304.
6. Wang CY. Boundary layers on rotating cones, disks and axisymmetric surfaces with concentrated heat source. *Acta Mech*. 1990;81(3-4): 245-251.
7. Fang T. Flow over a stretchable disk. *Phys Fluids*. 2007;19(12):128105.
8. Turkyilmazoglu M. MHD fluid flow and heat transfer due to a stretching rotating disk. *Int J Thermal Sci*. 2012;51:195-201.
9. Turkyilmazoglu M. MHD fluid flow and heat transfer due to a shrinking rotating disk. *Comput Fluids*. 2014;90:51-56.
10. Choi SUS. Enhancing thermal conductivity of fluids with nanoparticles. *ASME Int Mech Eng Congr Exp*. 1995;231:99-105.
11. Alsabery AI, Ghalambaz M, Armaghani T, Chamkha A, Hashim I, Saffari Pour M. Role of rotating cylinder toward mixed convection inside a wavy heated cavity via two-phase nanofluid concept. *Nanomater*. 2020;10(6):1138.
12. Noor NFM, Haq RU, Nadeem S, Hashim I. *Mixed Convection Stagnation flow of a Micropolar Nanofluid Along a Vertically Stretching Surface with Slip Effects*. Springer; 2015.

13. Khan WA, Aziz A, Uddin N. Buongiorno model for nanofluid Blasius flow with surface heat and mass fluxes. *J Thermophys Heat Transf*. 2013;1(27):134-141.
14. Ghalambaz M, Doostani A, Izadpanahi E, Chamkha AJ. Conjugate natural convection flow of Ag–MgO/water hybrid nanofluid in a square cavity. *J Thermal Anal Calorimetr*. 2020;139(3):2321-2336.
15. Mehryan SAM, Izadpanahi E, Ghalambaz M, Chamkha AJ. Mixed convection flow caused by an oscillating cylinder in a square cavity filled with Cu–Al_2O_3/water hybrid nanofluid. *J Thermal Anal Calorimetr*. 2019;137(3):965-982.
16. Mehryan SAM, Ghalambaz M, Chamkha AJ, Izadi M. Numerical study on natural convection of Ag–MgO hybrid/water nanofluid inside a porous enclosure: a local thermal non-equilibrium model. *Powder Technol*. 2020;367:443-455.
17. Fauzi ELA, Ahmad S, Pop I. Flow over a permeable stretching sheet in micropolar nanofluids with suction. *AIP Conf Proc*. 2014;1605:428-433.
18. Ghalambaz M, Mehryan SAM, Zahmatkesh I, Chamkha A. Free convection heat transfer analysis of a suspension of nano-encapsulated phase change materials (NEPCMs) in an inclined porous cavity. *Int J Thermal Sci*. 2020;157:106503.
19. Ghalambaz M, Chamkha AJ, Wen D. Natural convective flow and heat transfer of nano-encapsulated phase change materials (NEPCMs) in a cavity. *Int J Heat Mass Transf*. 2019;138:738-749.
20. Mehryan SAM, Ghalambaz M, Gargari LS, Hajjar A, Sheremet M. Natural convection flow of a suspension containing nano-encapsulated phase change particles in an eccentric annulus. *J Energy Stor*. 2020;28:101236.
21. Dinarvand S, Pop I. Free-convective flow of copper/water nanofluid about a rotating down-pointing cone using Tiwari-Das nanofluid scheme. *Adv Powder Technol*. 2017;28(3):900-909.
22. Eringen C. *Microcontinuum field thoeries, II. Fluent Media*. Springer.
23. Lukaszewicz G. *Micropolar fluids,theory and applications*. Springer; 1999.
24. Chen J, Liang C, Lee JD. Theory and simulation of micropolar fluid dynamics, Proceedings of the Institution of Mechanical Engineers. *Part N: J Nanoeng Nanosyst*. 2015;224:31-39.
25. Chen J, Lee JD, Liang C. Constitutive equations of micropolar electromagnetic fluids. *J Non-Newton Fluid Mech*. 2011;166(14-15):867-874.
26. Willson J. Boundary layers in micropolar liquids. *Math Proc Cambridge Philosophic Soc*. 1970;67(2):469-476.
27. Ahmadi G. Self-similar solution of incompressible micropolar boundary layer flow over a semi-infinite flat plate. *Int J Eng Sci*. 1976;14(7):639-646.
28. Chamkha AJ, Mohamed RA, Ahmed SE. Unsteady MHD natural convection from a heated vertical porous plate in a micropolar fluid with Joule heating, chemical reaction and radiation effects. *Mec Dent*. 2011;46(2):399-411.
29. Peddieson J. An application of the micropolar fluid model to the calculation of turbulent shear flow. *Int J Eng Sci*. 1972;10(1):23-32.
30. Khedr MEM, Chamkha AJ, Bayomi M. MHD flow of a micropolar fluid past a stretched permeable surface with heat generation or absorption. *Nonlin Anal Model Contr*. 2009;14(1):27-40.
31. Nawaz M. Two and three-dimensional flows of second grade and micropolar fluids, (2012).
32. Rashad AM, Abbasbandy S, Chamkha AJ. Mixed convection flow of a micropolar fluid over a continuously moving vertical surface immersed in a thermally and solutally stratified medium with chemical reaction. *J Taiwan Inst Chem Eng*. 2014;45(5):2163-2169.
33. Guram GS, Anwar M. Steady flow of a micropolar fluid due to a rotating disc. *J Eng Math*. 1979;3(13):223-234.
34. Hussain S, Kamal MA. Flow of micropolar fluids over a stretchable disk. *World Appl Sci J*. 2013;4(25):600-606.
35. Postelnicu A. Free convection about a vertical frustum of a cone in a micropolar fluid. *Int J Eng Sci*. 2006;44:672-682.
36. Takhar HS, Gorla RSR, Schore WR. Free convection boundary layer flow of a micropolar fluid past slender cones. *Mech Res Commun*. 1988;3(15):167-176.
37. Cheng CY. Natural convection of a micropolar fluid from a vertical truncated cone with power-law variation in surface temperature. *Int Commun Heat Mass Transf*. 2008;35(1):39-46.
38. Cheng CY. Natural convection boundary layer flow of a micropolar fluid over a vertical permeable cone with variable wall temperature. *Int Commun Heat Mass Transf*. 2011;38(4):429-433.
39. Gorla RSR, Nakamura S. Mixed convection of a micropolar fluid from a rotating cone. *Int J Heat Fluid Flow*. 1995;16:69-73.
40. Abo-Eldahab E, El Aziz A. Hall current and ohmic heating effects on mixed convection boundary layer flow of a micropolar fluid from a rotating cone with power-law variation in surface temperature. *Int J Heat Mass Transf*. 2004;31(5):751-762.
41. Gorla RS, Takhar HS. Boundary layer flow of micropolar fluid on rotating axisymmetric surfaces with a concentrated heat source. *Acta Mech*. 1994;105:1-10.
42. Ahmed SE. Modeling natural convection boundary layer flow of micropolar nanofluid over vertical permeable cone with variable wall temperature. *Appl Math Mech*. 2017;8(38):1171-1180.
43. Hussain ST, Nadeem S, Haq RU. Model-based analysis of micropolar nanofluid flow over a stretching surface. *Eur Phys J Plus*. 2014;129:161.
44. Subhani M, Nadeem S. Numerical analysis of 3D micropolar nanofluid flow induced by an exponentially stretching surface embedded in a porous medium. *Eur Phys J Plus*. 2017;132(10):441.

How to cite this article: Saleem A, Sabih W, Nadeem S, Ghalambaz M, Issakhov A. Theoretical aspects of micropolar nanofluid flow past a deformable rotating cone. *Math Meth Appl Sci*. 2020;1–19. https://doi.org/10.1002/mma.6777